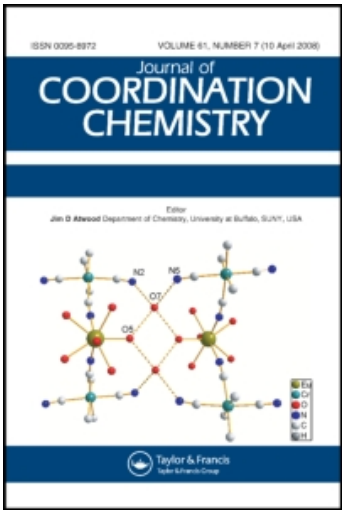


**Journal of Coordination Chemistry**
Publication details, including instructions for authors and subscription information:
http://www.informaworld.com/smpp/title~content=t713455674

# Spectroscopic characterization and biological activity of metal complexes with an ONO trifunctionalized hydrazone ligand

Abdou Saad El-Tabl[a]; Fathey A. El-Saied[a]; Ahmed Noman al-Hakimi[a]
[a] Faculty of Science, Department of Chemistry, Menoufia University, Shebin El-Kom, Egypt

Online publication date: 22 September 2010

**To cite this Article** El-Tabl, Abdou Saad , El-Saied, Fathey A. and al-Hakimi, Ahmed Noman(2008) 'Spectroscopic characterization and biological activity of metal complexes with an ONO trifunctionalized hydrazone ligand', Journal of Coordination Chemistry, 61: 15, 2380 — 2401
**To link to this Article: DOI:** 10.1080/00958970801914041
**URL:** http://dx.doi.org/10.1080/00958970801914041

*Journal of Coordination Chemistry*
Vol. 61, No. 15, 10 August 2008, 2380–2401

Taylor & Francis
Taylor & Francis Group

# Spectroscopic characterization and biological activity of metal complexes with an ONO trifunctionalized hydrazone ligand

ABDOU SAAD EL-TABL*, FATHEY A. EL-SAIED and AHMED NOMAN AL-HAKIMI

Faculty of Science, Department of Chemistry, Menoufia University, Shebin El-Kom, Egypt

(*Received 16 April 2007; in final form 28 August 2007*)



A series of Mn(II), Fe(III), Co(II), Ni(II), Cu(II), Zn(II), La(III), Ru(III), Hf(IV), Zr(IV) and U(VI) complexes of phenylamino acetoacetylacetone hydrazone have been synthesized and characterized by elemental analyses, IR, UV–Vis, magnetic moments, conductances, thermal analyses (DTA and TGA) and ESR measurements. The IR data show that the ligand is neutral bidentate, monobasic bidentate, monobasic tridentate or dibasic tridentate towards the metal ion. Molar conductances in DMF indicate that the complexes are non-electrolytes. The ESR spectra of solid $[(L)(HL)Cu_2(NO_3)(H_2O)]\cdot 1/2H_2O$ (**10**) and $[(H_2L)Cu(Cl)_2(H_2O)_2]$ (**11**) show axial spectra with $g_{\|} > g_{\perp} > 2.0023$ indicating $d_{(x^2-y^2)}$ ground state with significant covalent bond character. However, $[(HL)_2Mn_2(Cl)_2(H_2O)_4\cdot H_2O$ (**13**) shows an isotropic spectrum, indicating manganese(II) to be octahedral. Antibacterial and antifungal tests of the ligand and some of its metal complexes revealed that the complexes are more potent bactericides and fungicides than the ligand.

*Keywords*: Complexes; Spectroscopic studies; Conductivity; Thermal analyses; Syntheses; Magnetism; Biological activity

## 1. Introduction

Coordination chemistry of hydrazones has applications in antibacterial, antitumor and antitubercular activities [1, 2]. Hydrazones have been used as analytical reagents [3], as polymer-coating pigment [4] and fluorescent materials [5]. Synthesis and characterization of metal complexes of a bishydrazone derived from isatin monohydrazone and 2-hydroxyl-1-naphthaldehyde showed interesting biological properties [6, 7]. Transition metal complexes of salicylaldehyde thiazolyl hydrazone were prepared and characterized [8]. Acylhydrazones and their copper(II) complexes have been studied [9]. Dinuclear copper and iron complexes mimic bimetallic sites in various enzymes [10] and showed antifungal and antibacterial activities [11]. Metal(II) complexes of 2-acetylpyridine benzoylhydrazone were synthesized and

*Corresponding author. Email: asaeltabl@yahoo.com

*Journal of Coordination Chemistry*
ISSN 0095-8972 print/ISSN 1029-0389 online © 2008 Taylor & Francis
DOI: 10.1080/00958970801914041

crystallographically characterized [12]. Manganese(II), iron(III), nickel(II), cobalt(II) and zinc(II) complexes of 2,6-diformyl-4-methylphenoldibenzoylhydrazone have been prepared and characterized by elemental and spectroscopic measurements [13]. Cobalt(II), nickel(II), copper(II) and zinc(II) complexes of glyoxal bis(2-pyrazinoyl) hydrazone have also been prepared and characterized on the basis of analytical data and various physicochemical studies [14]. Mono-, di- or trinuclear dioxouranium complexes of vanillin benzoylhydrazone, salicylaldehyde benzoylhydrazone and 2-hydroxyacetyl benzene salicylhydrazone were prepared and characterized by elemental, X-ray analyses and spectroscopic measurements [15]. We now report the synthesis and characterterization of metal complexes of phenylamino acetoacetyl acetone hydrazone.

## 2. Experimental



Reagent grade chemicals were used. Phenylamino acetohydrazide was prepared by a published method [16]. Elemental analyses were determined by the Analytical Unit of Cairo University of Egypt. Standard methods were used to determine the metal ion content. All metal complexes were dried *in vacuo* over anhydrous $CaCl_2$. The IR spectra were measured using a Perkin-Elmer 683 spectrophotometer (4000–200 $cm^{-1}$). Electronic spectra in DMF were recorded on a Perkin-Elmer 550 spectrophotometer. The conductances of $10^{-3}$ M complexes in DMF were measured at 25°C with a Bibby conductometer type MCl. The $^1$H-NMR spectrum of the ligand in deuterated DMSO was recorded using a 300 MHz Varian NMR spectrometer. The thermal analyses (DTA and TGA) were carried out in air on a Shimadzu DT-30 thermal analyzer from 27 to 800°C at a heating rate of 10°C per minute. The magnetic moments of solid complexes were measured at room temperature with a Johnson Matthey magnetic susceptibility balance using $Hg[Co(SCN)_4]$ as a calibrant. Diamagnetic corrections were calculated from Pascal's constants [17]. All ESR measurements of solid samples at room temperature were made using a Varian E-109 spectrophotometer. DPPH was used as a standard.

### 2.1. *Preparation of [$H_2L$] (1) and its metal complexes*

**2.1.1. Preparation of [$H_2L$] (1).** Acetylacetone (1.1 g, 0.01 mol) was added dropwise to a solution of phenylaminoacetohydrazide (1.7 g, 0.01 mol) in 25 mL EtOH. The mixture was refluxed for 3 h and then left to cool to room temperature. The solid product was filtered off, washed several times with EtOH and dried over anhydrous $CaCl_2$.

**2.1.2. Preparation of metal complexes 2–5, 7, 9–10, 12–14, 16–18, 20–22, and 23.** These complexes were prepared by mixing stoichiometric ratios (1 : 1 or 2 : 1) of the ligand (30 mL EtOH) and metal salts (50 mL) in ethanol. The mixture was refluxed on a hot plate with stirring for 1–2 h, then a few drops of TEA (5 drops) were added. The mixture was heated for another 1 h. Cooling to room temperature, fine crystals

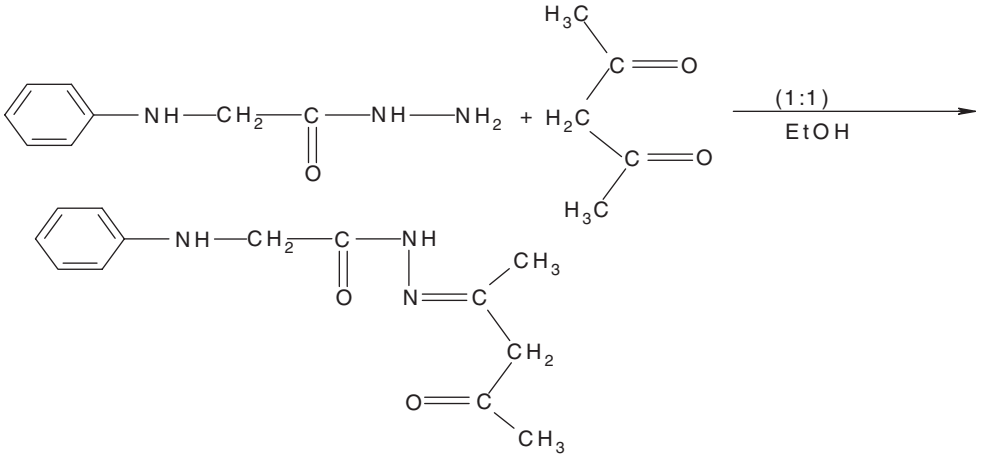


Scheme 1. Preparation of the ligand.



separated, were filtered off, washed several times with EtOH and dried over anhydrous $CaCl_2$.

**2.1.3. Preparation of metal complexes (6), (8), (11), (15), and (19).** These complexes were prepared by mixing stoichiometric ratios (1 : 1 or 2 : 1) of the ligand (30 mL EtOH) and metal salts (50 mL EtOH). The mixture was refluxed on a hot plate with stirring for 1–2 h. Upon cooling to room temperature the precipitate which formed was filtered off, washed several times with EtOH and dried over anhydrous $CaCl_2$.

## 2.2. *Microbiology*

**2.2.1. Fungus media.** Czapek dox agar medium was prepared by standard method [18]. *Aspergillus Niger* was spread over each dish by using a sterile bent Loop rod. Disks were cut by a sterilized cork borer and then taken by sterilized needle. The resulting pits are sites for the tested compounds. The plates are incubated at 30°C for 24–48 h and then any clear zones present were detected.

**2.2.2. Bacteria media.** Nutrient agar medium was prepared by standard method [18]. *E. coli* was spread over each dish by using a sterile bent Loop rod. Disks were cut by a sterilized cork borer and then taken by sterilized needle. The resulting pits are sites for the tested compounds. The plates are incubated at 37°C for 24–48 h and then any clear zones present were detected.

## 3. Results and discussion

Reaction of phenyl amino acetohydrazide with acetylacetone in EtOH 1 : 1 molar ratio led to formation of $H_2L$ (**1**), as shown in scheme 1.

The IR spectra of the ligand and its metal complexes show that the ligand has tautomeric forms (I–III), as shown below:

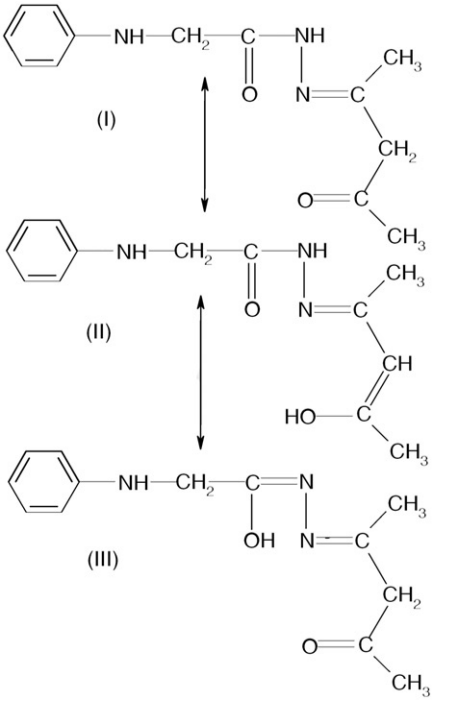


Reaction of **1** with metal salts using (1 : 1) or (2 : 1) molar ratios in the presence of triethylamine gives **2**, **3**, **4**, **5**, **7**, **9**, **10**, **12**, **13**, **14**, **16**, **17**, **18**, **20**, **21**, **22** and **23**, however, in the absence of triethylamine it gives complexes **6**, **8**, **11**, **15** and **19** with different geometries. The reactions leading to complexes **2**–**23** are represented schematically in scheme 2.

The new complexes are intensely colored, crystalline solids stable at room temperature and insoluble in non polar and polar solvents but soluble in polar coordinating solvents such as DMSO and DMF. Elemental analyses, physical data (table 1), and spectral data (tables 2 and 3) are compatible with the suggested structures, as shown in figure 1. Reaction of **7** and **14** with acetylacetone (1 : 1 molar ratio) in ethanol led to formation of **8** and **15**, respectively.

### 3.1. *$^1$H-NMR spectrum*

The $^1$H-NMR spectrum of $H_2L$ in deuterated DMSO shows signals consistent with the proposed structure. The peaks at 7.05–7.1 ppm are assignable to the NH proton [19]. Multiplets at 6.20–6.62 ppm are due to aromatic protons. The resonances at 4.63 and 2.46 ppm are due to methylene and methyl groups, respectively [12, 19, 20]. The zinc(II) complex **19** shows peaks at 6.5–6.92 ppm due to NH protons and the aromatic protons are at 5.78–5.88 ppm. The methylene and methyl groups are observed at 3.58 and 2.4 ppm [12, 19, 20]. The shift of the peaks to lower values indicate that coordination occurred.

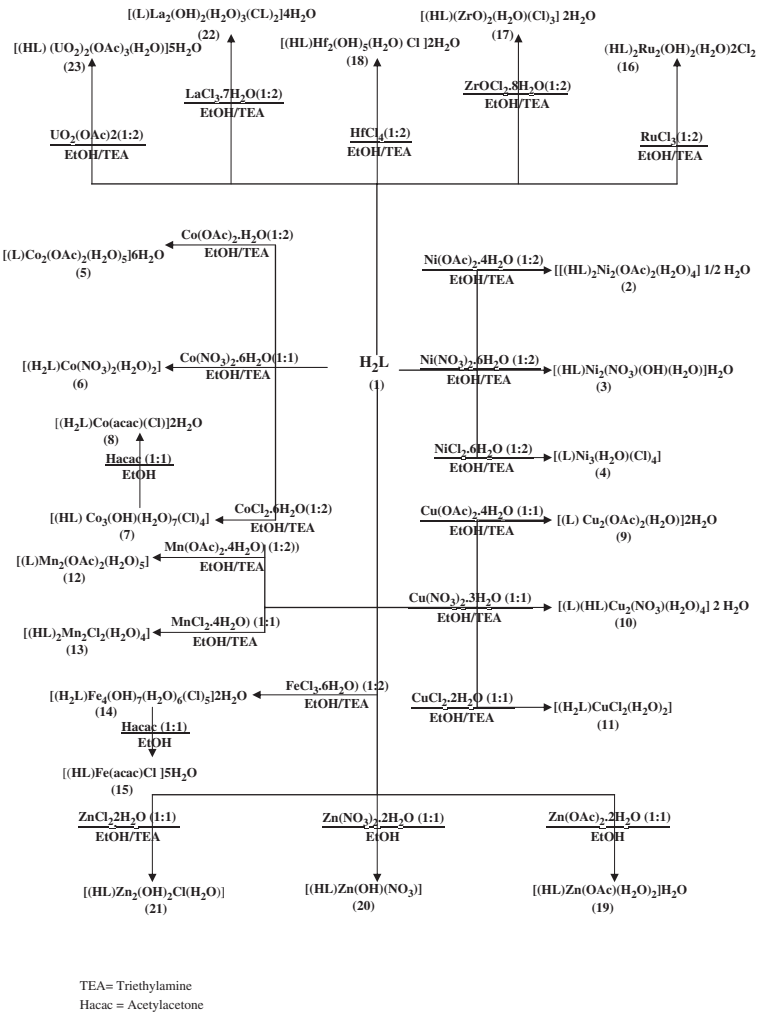


Scheme 2. Preparation of the metal complexes.

### 3.2. *Conductivity measurements*

The molar conductance values of the complexes in DMF ($10^{-3}$ M) are in the 1.3–12.4 $\Omega^{-1}\,cm^2\,mol^{-1}$ range (table 1); the low values indicate non-electrolytic complexes [21], confirming that the anion is coordinated to the metal.

### 3.3. *IR spectra*

The bonding of the ligand to the metal has been deduced from IR spectra. Important spectral bands of the ligand and metal complexes are presented in table 2. The IR spectrum of the ligand shows broad medium bands in the 3510–3200 and 3185–2580 $cm^{-1}$ ranges, attributed to intra- and intermolecular hydrogen bonds. The two bands indicate two types of hydrogen bonds, the higher frequency band

Table 1. Elemental analyses and physical properties of $H_2L$ **(1)** and its metal complexes.

| No. | Molecular formula | Color | M.P. (°C) | Yield% | $\Omega^{-1}$ $cm^2 mol^{-1}$ | $\mu_{eff}$ (B.M.) | Found (Calcd)% | | | | |
|---|---|---|---|---|---|---|---|---|---|---|---|
| | | | | | | | C | H | N | Cl | M |
| (1) | $[H_2L]$ $[C_{13}H_{17}N_3O_2]$ | White | 100 | 86 | – | – | 63.5(63.2) | 5.9(6.0) | 17.0(17.1) | – | – |
| (2) | $[(HL)_2Ni_2(OAc)_2(H_2O)_4]$ $1/2H_2O$ $[C_{30}H_{46}N_6O_{12}Ni_2]1/2H_2O$ | Green | 200 | 75 | 4.2 | 2.3 | 44.59(44.5) | 5.7(5.8) | 10.4(10.3) | – | 14.9(14.6) |
| (3) | $[(HL)Ni_2(NO_3)(OH)(H_2O)]H_2O$ $[C_{13}H_{21}N_5O_{11}Ni_2]$ | Green | 160 | 76 | 8.3 | Dia | 28.8(28.9) | 3.7(3.9) | 12.5(13.0) | – | 21.5(21.7) |
| (4) | $[(L)Ni_3(H_2O)(Cl)_4]$ $[C_{13}H_{25}N_3O_7Ni_3Cl_4]$ | Pale green | 240 | 70 | 7.5 | Dia | 23.8(23.9) | 3.5(3.8) | 6.3(6.4) | 22.0(21.8) | 26.7(27.0) |
| (5) | $[(L)Co_2(OAc)_2(H_2O)_5]6H_2O$ $[C_{17}H_{43}N_3O_{17}Co_2]$ | Violet | 180 | 75 | 2.1 | 3.9 | 28.5(29.3) | 5.8 (6.2) | 6.0(6.0) | – | 17.0(17.0) |
| (6) | $[(H_2L)Co(NO_3)_2(H_2O)_2]$ $[C_{13}H_{21}N_5O_{10}Co]$ | Violet | 220 | 80 | 4.1 | 4.9 | 33.5(33.5) | 4.5(4.5) | 15.1(15.0) | – | 12.6(12.7) |
| (7) | $[(HL)Co_3(OH)(H_2O)_7(Cl)_4]$ $[C_{13}H_{31}N_3O_{10}Co_3Cl_4]$ | Violet | >300 | 65 | 6.2 | 2.8 | 22.4(22.0) | 4.3(4.4) | 5.7(6.0) | 20.5(20) | 25.1(25) |
| (8) | $[(H_2L)Co(acac)(Cl)]2H_2O$ $[C_{18}H_{27}N_3O_6Cl]$ | Green | 110 | 68 | 3.8 | 4.08 | 44.6(45.4) | 5.6(5.7) | 8.9(8.8) | 7.6(7.5) | 12.4(12.4) |
| (9) | $[(L)Cu_2(OAc)_2(H_2O)]2H_2O$ $[C_{17}H_{27}N_3O_9Cu_2]$ | Green | 235 | 77 | 4.5 | 1.25 | 37.9(37.5) | 4.6(5.0) | 7.8(7.7) | – | 23.8(23.4) |
| (10) | $[(L)(HL)Cu_2(NO_3)(H_2O)_4]1/2H_2O$ $[C_{26}H_{39}N_7O_{11}Cu_2]1/2H_2O$ | Dark green | 200 | 80 | 3.2 | 1.3 | 41.28(41.0) | 5.2(5.3) | 13.0(12.9) | – | 17(16.7) |
| (11) | $[(H_2L)CuCl_2(H_2O)_2]$ $[C_{13}H_{21}N_3O_4CuCl_2]$ | Dark green | 210 | 83 | 3.2 | 1.77 | 37.8(37.3) | 5.0(5.0) | 10.1 (10.0) | 17(17.0) | 15.5(15.2) |
| (12) | $[(L)Mn_2(OAc)_2(H_2O)_5]$ $[C_{17}H_{31}N_3O_{11}Mn_2]$ | Brown | >300 | 73 | 6.7 | 3.6 | 36.5(36.2) | 5.5(5.5) | 7.8(7.5) | – | 19.5(19.5) |
| (13) | $[(HL)_2Mn_2Cl_2(H_2O)_4]H_2O$ $[C_{26}H_{42}N_6O_9Mn_2Cl_2]$ | Yellowish brown | 260 | 74 | 9.3 | 3.4 | 40.6(41.0) | 5.3(5.5) | 11.2(11.0) | 9.53(9.3) | 14.8(14.4) |

(*Continued*)

Table 1. Continued.

| No. | Molecular formula | Color | M.P. (°C) | Yield% | $\Omega^{-1}$ $cm^2 mol^{-1}$ | $\mu_{eff}$ (B.M.) | Found (Calcd)% | | | | |
|---|---|---|---|---|---|---|---|---|---|---|---|
| | | | | | | | C | H | N | Cl | M |
| (14) | $[(H_2L)Fe_4(OH)_7(H_2O)_6(Cl)_5]2H_2O$ $[C_{13}H_{36}N_3O_{15}Fe_4Cl_5]$ | Brown | >300 | 66 | 5.3 | 3.2 | 17.6(17.8) | 4.2(4.1) | 4.7(4.8) | 20.4(20.3) | 25.7(25.5) |
| (15) | $[(HL)Fe(acac)Cl]5H_2O$ $[C_{18}H_{33}N_3O_9FeCl]$ | Red | 135 | 70 | 12.4 | 5.74 | 41.9(41.1) | 6.3(6.3) | 8.0(8.0) | 6.7(6.8) | 10.7(10.6) |
| (16) | $[(HL)_2Ru_2(OH)_2(H_2O)_2Cl_2]$ $[C_{26}H_{44}N_6O_{11}Ru_2Cl_2]$ | Black | 120 | 76 | 2.1 | 1.5 | 35.0(35.1) | 5.0(5.0) | 9.5(9.5) | 8.0(8.0) | 22.8(22.7) |
| (17) | $[(HL)(ZrO)_2(H_2O)(Cl)_3]2H_2O$ $[C_{13}H_{22}N_3O_7Zr_2Cl_3]$ | Dark green | >300 | 80 | 3.2 | Dia. | 25.1(25.1) | 4.1(3.6) | 6.8(6.8) | 17.4(17.2) | 29.7 (29.4) |
| (18) | $[(HL)Hf_2(OH)_5(H_2O)Cl]2H_2O$ $[C_{13}H_{27}N_3O_{10}Hf_2Cl_2]$ | Dark green | >300 | 79 | 4.2 | Dia | 19.6(19.2) | 3.3(3.3) | 5.3(5.2) | 8.8(8.7) | 43.8(43.8) |
| (19) | $[(HL)Zn(OAc)(H_2O)_2]H_2O$ $[C_{15}H_{25}N_3O_7Zn]$ | Pale yellow | 125 | 82 | 1.4 | Dia | 42.7(42.7) | 6.6(6.0) | 10(10) | – | 15.8(15.5) |
| (20) | $[(HL)Zn(OH)(NO_3)]$ $[C_{13}H_{18}N_4O_6Zn]$ | White | 175 | 80 | 1.22 | Dia | 39.5(40.0) | 4.7(4.4) | 14.4(14.4) | – | 16.9(16.7) |
| (21) | $[(HL)Zn_2(OH)_2Cl(H_2O)]$ $[C_{13}H_{21}N_3O_5Zn_2Cl]$ | White | >300 | 78 | 1.3 | Dia | 33.7(33.5) | 4.6(4.5) | 9.0(9.0) | 7.7(7.6) | 28.2(28.1) |
| (22) | $[(L)La_2(OH)_2(H_2O)_3(CL)_2]4H_2O$ $[C_{13}H_{31}N_3O_{11}La_2Cl_2]$ | Orange | 190 | 70 | 2.3 | Dia | 21.0(21.0) | 5(4.1) | 5.7(5.6) | 9.7(9.4) | 37(36.9) |
| (23) | $[(HL)(UO_2)_2(OAc)_3(H_2O)]5H_2O$ $[C_{19}H_{37}N_3O_{18}U_2]$ | Orange | 165 | 72 | 3.2 | Dia | 21.0(21.0) | 3.7(3.5) | 4.1(4.0) | – | 44.5(44.4) |

Table 2. IR spectra (assignments) of $H_2L$ (**1**) and its metal complexes.

| No. | ν(lattice$H_2O$) /(OH) | ν(Coord. $H_2O$) | ν(H-bond) | ν(NH) | ν(C=O) | ν(C=N) | ν(C=C)$_{Ar}$ | ν(CH=C)$_{Al}$ | ν(C–O) | ν(OAc) | ν($NO_3$) | ν(M–O) | ν(M–N) | ν(M–Cl) |
|---|---|---|---|---|---|---|---|---|---|---|---|---|---|---|
| (1) | – | – | 3510–3200<br>3185–3580 | 3405, 3108 | 1718 | 1605 | 1589 | 1513 | 1326 | – | – | – | – | – |
| (2) | 3650–3300 | 3260–3080<br>860 | 3600–3050<br>3000–2560 | 3248, 3160 | 1716 | 1613 | 1600 | 1530 | 1350 | 1570, 1418 | – | 614 | 535 | – |
| (3) | 3600–3280<br>3640 | 3240–2980<br>826 | 3620–2980<br>2970–2500 | 3405, 3250 | 1763 | 1615 | 1605 | 1532 | 1270 | – | 1490, 1386<br>1178, 826, 758 | 659 | 629 | – |
| (4) | 3660–3270 | 3250–3000<br>810 | 3600–3000<br>2990–2650 | 3398, 3225 | – | 1620 | 1594 | 1515 | 1316 | – | – | 694 | 590 | 425, 370 |
| (5) | 3650–3265 | 3260–2980<br>800 | 3620–3100<br>3000–2560 | 3418, 3225 | – | 1608 | 1561 | 1527 | 1321 | 1600, 1400<br>1561, 1414 | – | 659 | 520 | – |
| (6) | – | 3420–3270<br>827 | 3600–3200<br>3180–2500 | 3390, 3265 | 1739 | 1604 | 1590 | – | 1320 | – | 1382,<br>1216, 827, 752 | 693 | 510 | – |
| (7) | –<br>3552 | 3380–3180<br>839 | 3480–3000<br>2990–2620 | 3285, 3175 | 1736 | 1618 | 1602 | 1522 | 1318 | – | – | 696 | 508 | 380 |
| (8) | 3580–3270 | – | 3600–3100<br>3080–2650 | 3434, 3150 | 1699 | 1620 | 1585 | 1520 | 1320 | – | – | 693 | 501 | 420 |
| (9) | 3610–3275 | 3250–3115<br>767 | 3580–3150<br>3100–2600 | 3422 | – | 1649, 1615 | 1574 | 1523 | 1346 | 1615, 1378<br>1565, 1422 | – | 689, 650 | 617 | – |
| (10) | 3580–3270 | 3450–3230<br>834 | 3600–3200<br>3190–2500 | 3402, 3245 | 1732 | 1640, 1613 | 1590 | 1522 | 1275 | – | 1466, 1370<br>1180, 830, 765 | 619 | 512 | – |
| (11) | – | 3270–2750<br>806 | 3550–3240<br>3150–2480 | 3422, 3267 | 1726 | 1622 | 1600 | – | – | – | – | 693, 615 | 513 | 417 |
| (12) | – | 3260–2960<br>813 | 3580–3210<br>3200–2650 | 3406 | – | 1640, 1596 | 1567 | 1513 | 1320 | 1600, 1410<br>1580, 1400 | – | 614 | 604 | – |
| (13) | 3520–3150 | 3200–3000<br>820 | 3600–3200<br>3190–2700 | 3385, 3267 | 1732 | 1605 | 1572 | 1520 | 1273 | – | – | 687, 660 | 605, 512 | 417, 350 |
| (14) | 3565–3245<br>3500 | – | 3600–3240<br>3235–2485 | 3394, 3200 | 1702, 1651 | 1614 | 1596 | – | – | – | – | 665, 642 | 555 | 415, 360 |

(*Continued*)

Table 2. Continued.

| No. | $\nu$(lattice$H_2O$) /(OH) | $\nu$(Coord. $H_2O$) | $\nu$(H-bond) | $\nu$(NH) | $\nu$(C=O) | $\nu$(C=N) | $\nu(C=C)_{Ar}$ | $\nu(CH=C)_{Al}$ | $\nu$(C–O) | $\nu$(OAc) | $\nu(NO_3)$ | $\nu$(M–O) | $\nu$(M–N) | $\nu$(M–Cl) |
|---|---|---|---|---|---|---|---|---|---|---|---|---|---|---|
| (15) | 3610–3240 | – | 3600–3180<br>3175–2650 | 3424, 3200 | 1680 | 1614 | 1570 | 1525 | 1365 | – | – | 668 | 554 | 420 |
| (16) | 3630–3260 | 3250–2870<br>828 | 3620–3165<br>3150–2465 | 3419, 3200 | 1708 | 1616 | 1598 | 1526 | 1332 | – | – | 697 | 511 | 421, 380 |
| (17) | 3650–3150 | – | 3630–3130<br>3125–2450 | 3388, 3235 | 1734 | 1610 | 1580 | 1516 | 1235 | – | – | 669 | 507 | 415, 370 |
| (18) | 3600–3240 | 3235–2950<br>825 | 3630–3125<br>3120–2435 | 3402, 3245 | 1732 | 1640, 1613 | 1590 | 1522 | 1275 | – | – | 619 | 525 | 415 |
| (19) | 3580–3230 | 3225–2930<br>753 | 3570–3135<br>3130–2625 | 3349, 3231 | – | 1605 | 1565 | 1530 | 1341 | 1576, 1407 | – | 694 | 504 | |
| (20) | 3690 | – | 3600–3185<br>3180–2680 | 3396, 3250 | 1743 | 1605 | 1578 | 1530 | 1338 | – | 1383<br>1216, 812, 755 | 694 | 539, 504 | – |
| (21) | 3691 | 3410–3115<br>780 | 3625–3180<br>3175–2685 | 3406, 3215 | 1745 | 1604 | 1572 | 1529 | 1342 | – | – | 692 | 520 | 416 |
| (22) | 3550–3260 | 3250–3000<br>838 | 3580–3240<br>3225–2485 | 3407 | – | 1627, 1615 | 1600 | 1510 | 1315, 1252 | – | – | 694 | 542 | 420 |
| (23) | 3625–3250 | 3235–2990<br>755 | 3610–3200<br>3175–2460 | 3400, 3143 | 1744 | 1625 | 1546 | 1505 | 1309 | 1605, 1400<br>1570, 1411 | – | 694 | 500 | – |

Table 3. UV-Vis spectra of $H_2L$ **(1)** and its metal complexes.

| No. | $\lambda_{max}$ (nm) |
|---|---|
| (1) | 320 ($\epsilon = 7.7 \times 10^3\,mol^{-1}\,cm^{-1}$) |
| | 270 ($\epsilon = 6.5 \times 10^3\,mol^{-1}\,cm^{-1}$) |
| (2) | 850, 620, 490, 315, 265 |
| (3) | 570, 475, 290, 250 |
| (4) | 550, 450, 295, 255 |
| (5) | 660, 550, 385, 290 |
| (6) | 645, 580, 400, 315, 250 |
| (7) | 650, 550, 390, 310, 245 |
| (8) | 670, 560, 390, 315, 255 |
| (9) | 600, 420, 390, 310, 230 |
| (10) | 600, 480, 395, 315, 260 |
| (11) | 665, 490, 435, 310, 230 |
| (12) | 580, 480, 285, 255 |
| (13) | 680, 545, 480, 310, 240 |
| (14) | 660, 550, 460, 300, 255 |
| (15) | 665, 490, 445, 310, 260 |
| (16) | 620, 410, 300, 255 |
| (17) | 420, 310, 255 |
| (18) | 420, 310, 255 |
| (19) | 315, 220 |
| (20) | 315, 220 |
| (21) | 305, 220 |
| (22) | 315, 240 |
| (23) | 445, 310, 250 |



(3510–3200 $cm^{-1}$) is associated with a weaker hydrogen bond between –OH and >C=N groups in the same molecule and the lower frequency band (3185–2580 $cm^{-1}$) is from stronger hydrogen bond between –NH or –OH and >C=O or >C=N of different molecules [22, 23]. The spectrum shows bands at 3405, 3108, 1718 and 1605 $cm^{-1}$, assigned to secondary $\nu$(NH), $\nu$(C=O) and $\nu$(C=N), respectively [24–26]. Bands at 1589, 1513 and 1326 $cm^{-1}$ correspond to $\nu(C{=}C)_{Ar}$, $\nu(CH{=}C)_{Al}$ and $\nu$(C–O), respectively [25, 27]. The complexes show a broad band from lattice water at 3660–3150 $cm^{-1}$, except **6**, **7**, **11**, **12**, **20** and **21**; coordinated water appears at 3450–2750 $cm^{-1}$ except in **8**, **15**, **17** and **20** [27–29]. Two types of hydrogen bonds (intra- and intermolecular) are observed at 3630–3000 and 3235–2435 $cm^{-1}$ in **2**–**23** [26–28], (table 2). However, the secondary $\nu$(NH) appears at 3434–3248 and 3267–3143 $cm^{-1}$, except for **9**, **12** and **22** [27, 29]. The complexes show a band between 1763–1651 $cm^{-1}$ (table 2), assigned to $\nu$(C=O) [30, 31] and bands between 1649–1604, 1605–1546 and 1532–1505 $cm^{-1}$ are due to $\nu$(C=N), $\nu(C{=}C)_{Ar}$ and $\nu$(CH=C), respectively [25, 32]. The shift of these bands indicates coordination. Complexes **3**, **7**, **14**, **20** and **21** show a band at 3691–3500 $cm^{-1}$, due to coordinated $\nu$(OH) group, and bridging $\nu$(OH) is observed at 981–826 $cm^{-1}$ for **14**, **16**, **18**, **21** and **22** (table 2) [29]. Extensive IR spectral studies reported on metal acetato complexes [33] indicate that the acetato ligand coordinates in either a monodentate, bidentate or bridging manner. The $\nu_a(CO_2)$ and $\nu_s(CO_2)$ of the free acetate are at 1560 and 1416 $cm^{-1}$, respectively. In monodentate coordination $\nu$(C=O) is at higher energy than $\nu_a(CO_2)$ and $\nu$(C–O) is lower than $\nu_s(CO_2)$. As a result, the separation between $\nu$(CO) bands is much larger in monodentate complexes. In **5**, **9**, **12**, **19** and **23** the $\nu_a(CO_2)$=1600, 1615, 1600, 1576 and 1605 $cm^{-1}$ and $\nu_s(CO_2)$=1400, 1378, 1410, 1407 and 1400 $cm^{-1}$, respectively, however, bridging acetate group with both

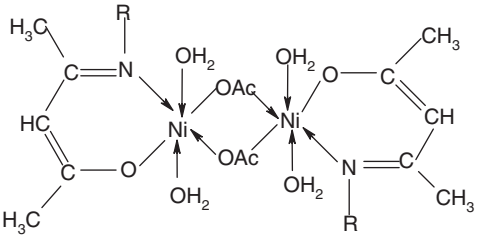


· 1/2 $H_2O$

R = NH-CO-$CH_2$-NH-ph (**2**)

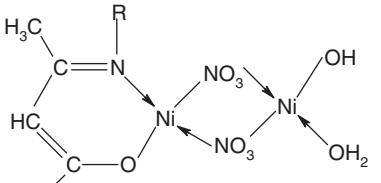


· $H_2O$

R= NH-CO-$CH_2$-NH-ph (**3**)

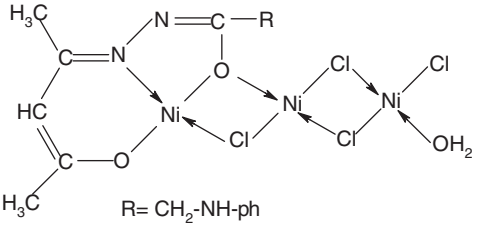


· 4 $H_2O$

R= $CH_2$-NH-ph (**4**)

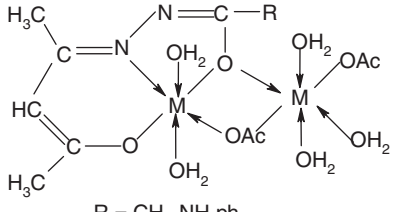


· n $H_2O$

R = $CH_2$-NH-ph

M = Co, n = 6 (**5**)
M = Mn, n = 0 (**12**)

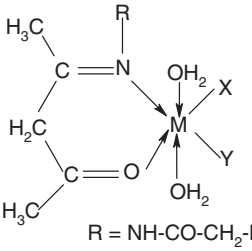


M = Co, X=Y=$NO_3$ (**6**)
M = Cu, X=Y=Cl (**11**)

R = NH-CO-$CH_2$-NH-ph

Figure 1. Structure representations of the metal complexes.

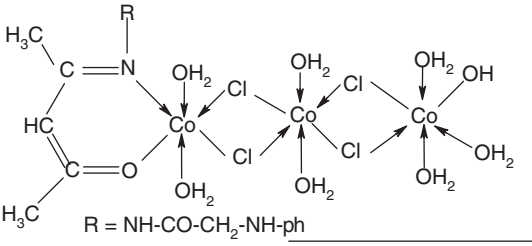


R = NH-CO-$CH_2$-NH-ph (**7**)

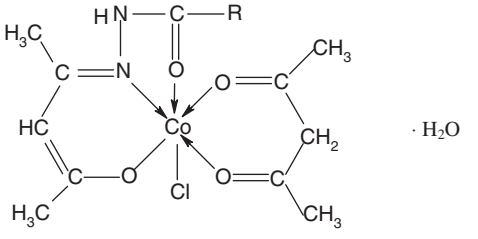


· $H_2O$

R = $CH_2$-NH-ph (**8**)

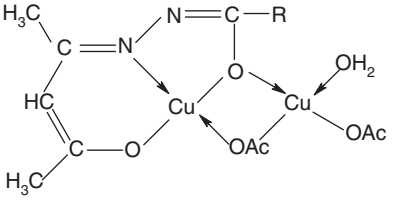


· $2H_2O$

R = $CH_2$-NH-ph (**9**)

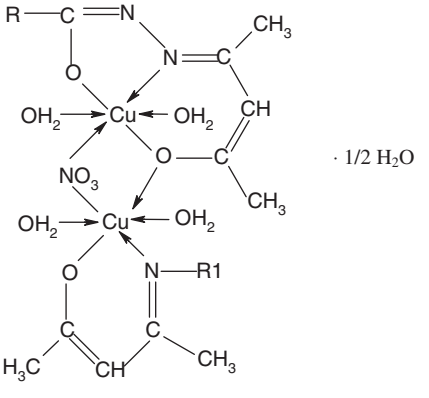


· 1/2 $H_2O$

R = $CH_2$-NH-pH
$R_1$= NH-CO-$CH_2$-NH-PH (**10**)

Figure 1. Continued.

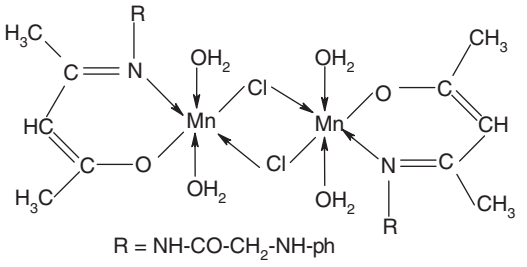


· $H_2O$

(**13**)

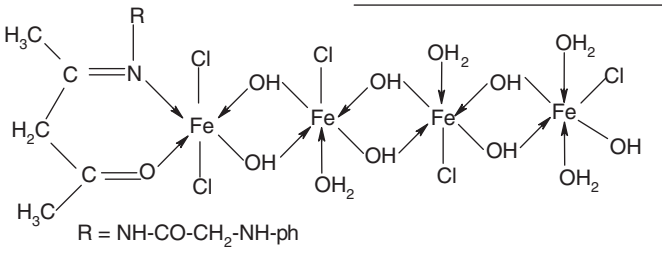


· $2H_2O$

(**14**)

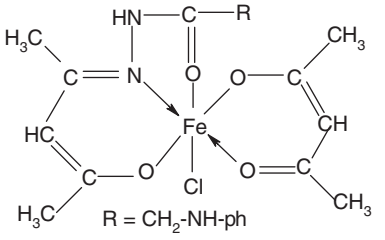


· $5H_2O$

(**15**)

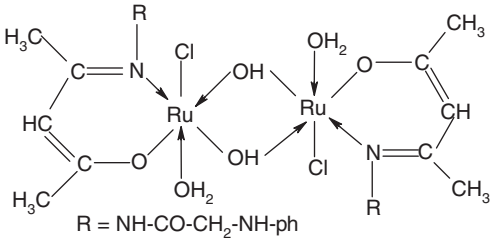


· $3H_2O$

(**16**)

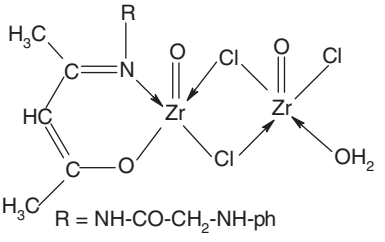


· $2H_2O$

(**17**)

Figure 1. Continued.

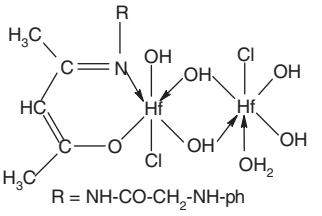


$2H_2O$

(**18**)

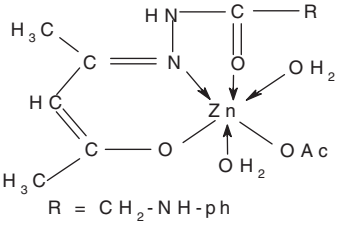


$\cdot H_2O$

(**19**)

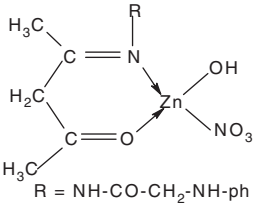


(**20**)

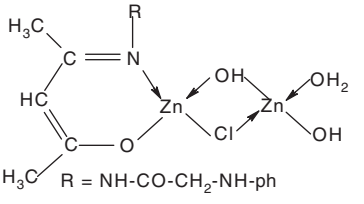


(**21**)

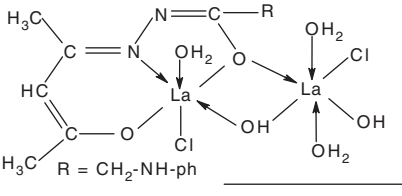


$\cdot 4H_2O$

(**22**)

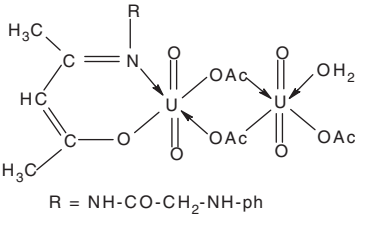


$\cdot 5H_2O$

(**23**)

Figure 1. Continued.

oxygens coordinated (as in copper(II) acetate) have $\nu$(CO) bands close to the free ion values [29, 34], as found for **2**, **5**, **9**, **12** and **23** (*i.e.*, $\nu_a(CO_2)$=1570, 1561, 1565, 1580 and 1570 $cm^{-1}$), $\nu_s(CO_2)$=1418, 1414, 1422, 1400 and 1411 $cm^{-1}$. Complexes **3** and **10** show bands at 1490, 1386, 1178, 826, 758, 1466, 1370, 1180, 830, and 765 $cm^{-1}$, and complexes **6** and **20** show bands at 1382, 1216, 827, 752, 1383, 1216, 812, and 755 $cm^{-1}$, respectively (table 2), assigned to bridging and terminal nitrate [29, 33, 35, 36]. The band at 1350–1245 $cm^{-1}$, except for **12** and **14**, is from $\nu$(CO) [27, 29]. Complexes **4**, **14**, **16** and **17** show bands at 370 and 380 $cm^{-1}$ and in the 425–421 $cm^{-1}$ range corresponding to bridging and terminal chlorides; complexes **7** and **13** show bands at 380 and 365 $cm^{-1}$ indicating a bridging chloride; **8**, **11**, **15**, **18**, **21** and **22** show a band at 420–415 $cm^{-1}$, assigned to terminal chloride [29, 37]. Complex **23** shows a band at 918 $cm^{-1}$ due to O=U=O [38]. The bonding of metal to ligand through the oxygen and nitrogen atoms is supported by the presence of new bands in the 694–614 and 629–501 $cm^{-1}$ ranges, due to $\nu$(M–O) and $\nu$(M–N), respectively [33, 39].

The above results together with the elemental analysis indicate that the hydrazone is a neutral bidentate (**6**, **7**, **11**, **14**, **20**), monobasic bidentate (**2**, **3**, **13**, **16**–**18**, **21**, **23**), monobasic tridentate (**8**, **15**, **19**) or dibasic tridentate (**4**, **5**, **9**, **10**, **12**, **22**) ligand via the carbonyl oxygen of the hydrazide moiety, carbonyl oxygen of the acetylacetone moiety in enolic or ketonic form and azomethine nitrogen atom.



### 3.4. *Magnetic moment*

The room temperature magnetic moments of **2**–**23** are presented in table 1. Ni(II) complex **2** gave moments of 2.3 B.M., indicating octahedral geometry. The low moments indicate spin exchange interactions take place between the Ni(II) ions through the acetate group. Complexes **3** and **4** are diamagnetic confirming square planar geometry around Ni(II) [38–40]. Cobalt(II) complexes **5**–**8** gave moments in the 4.9–3.9 B.M. range (table 1), indicating high spin octahedral complexes [19]. The magnetic moments for the copper(II) complexes **9**, **10** and **11** are 1.2, 1.3 and 1.77 B.M.; for **9** and **10**, the moments are well below the spin-only moment (1.73 B.M.), indicating spin-exchange interactions between the copper(II) ion in a square planar or octahedral geometry [39]. The moment of **11** corresponds to one unpaired electron in an octahedral structure [19]. The magnetic moment values for **12** and **13** are 3.6 and 3.4 B.M. suggesting octahedral geometry around manganese(II) [19]. The low moments may be ascribed to superexchange which takes place between manganese(II) ions. Iron(III) complex **14** has a moment of 3.2 B.M., and the reduced magnetic moment may result from spin density exchange between the iron(III) centers in an octahedral structure, Complex **15** has a moment of 5.74 B.M., indicating high spin octahedral iron(III) [6]. Ruthenium(III) complex **16** gave a magnetic moment of 1.5 B.M., well below the spin only moment, indicating spin-exchange interactions between ruthenium(III) ions through the hydroxyl group in octahedral structure [41]. Zirconium(IV) complex **17**, hafnium(IV) complex **18**, zinc(II) complexes **19**–**21**, lanthanum(III) complex **22** and uranyl complex **23** are diamagnetic.

### 3.5. *Electronic spectra*

The electronic spectral data of the ligand **1** and its metal complexes in DMF solution are presented in table 3. Complex **2** shows bands at 490, 620 and 850 nm, attributable to $^3A_{2g}(F) \rightarrow {}^3T_{1g}(P)$ ($\upsilon_3$), $^3A_{2g}(F) \rightarrow {}^3T_{1g}(F)$ ($\upsilon_2$) and $^3A_{2g}(F) \rightarrow {}^3T_{2g}(F)$ ($\upsilon_1$) transitions, respectively, indicating octahedral nickel(II) [42]. The $\upsilon_2/\upsilon_1$ ratio for **2** is 1.37 which is less than the usual range of 1.5–1.75, indicating distorted octahedral nickel(II) [43]. However, **3** and **4** show bands at 475 and 570 nm and 450 and 550 nm, respectively, assigned to $^3T_1 \rightarrow {}^3T_2$ and $^3T_1(F) \rightarrow {}^3T_2(P)$ transitions, indicating square planar nickel(II) [38, 44]. Complexes **5**, **6**, **7** and **8** show bands in the 400–385, 580–550 and 670–645 nm ranges, assigned to $^4T_{1g}(F) \rightarrow {}^4T_{1g}(P)$, $^4T_{1g}(F) \rightarrow {}^4A_{2g}$ and $^4T_{1g}(F) \rightarrow {}^4T_{2g}(F)$ transitions, respectively, corresponding to high spin octahedral cobalt(II) [40, 45]. Copper(II) complexes **9**, **10** and **11** show different bands (table 3). Complex **9** shows bands at 390, 420 and 600 nm, corresponding to $^2B_{1g} \rightarrow {}^2B_{2g}$, $^2B_{1g} \rightarrow {}^2E_g$ and $^2B_{1g} \rightarrow {}^2A_{1g}$ transitions, respectively, suggesting a square-planar geometry [46]. However, **10** and **11** show bands at 395, 480 and 600 nm and 435, 490 and 665 nm, respectively, assigned to ligand $\rightarrow$ metal charge transfer, $^2B_1 \rightarrow {}^2E$ and $^2B_1 \rightarrow {}^2B_2$ transitions, indicating distorted octahedral structures [9, 43, 47]. Complexes **12** and **13** show bands at 480, 580 and 665 nm and 480, 545 and 680 nm, respectively, corresponding to $^6A_{1g} \rightarrow {}^4E_g$, $^6A_{1g} \rightarrow {}^4T_{2g}$ and $^6A_{1g} \rightarrow {}^4T_{1g}$ transitions, compatible to octahedral geometry around manganese(II) [48]. Complexes **14** and **15** show bands at 460, 550 and 660 nm and 445, 490 and 665 nm, respectively. The first two bands are due to charge transfer transition while the last band arises from the $^6A_1 \rightarrow {}^4T_1$ transition, suggesting distorted octahedral geometry around the iron(III) [47, 49]. Complex **16** shows bands at 410 and 620 nm, the first due to LMCT and the second to $^2T_{2g} \rightarrow {}^2A_{2g}$. The band positions are similar to those observed for other octahedral ruthenium(III) complexes [50, 51]. Zirconium(IV) complex **17**, hafnium(IV) complex **18**, zinc(II) complexes **19**, **20** and **21**, lanthanum(III) complex **22**, and uranyl(VI) complex **23** show bands (table 3) indicating intraligand transitions [49, 52, 53].



### 3.6. *Electron Spin Resonance (ESR)*

The ESR spectra of solid copper(II) complexes **10** and **11** at room temperature have axial symmetry of a $d_{(x^2-y^2)}$ ground state [54]. The g-values suggest octahedral geometry [30] and the complexes show $g_\parallel > g_\perp > 2.0023$, indicating tetragonal distortion around the copper(II) ion [22, 55, 56]. The ESR parameters for **10** are $g_\parallel = 2.27$, $g_\perp = 2.09$ and $g_{iso} = 2.15$, $A_\parallel = 150$ G, $A_\perp = 30$ G and $A_{iso} = 70$ G, $G = 3.0$, $A_\parallel = 0.0159\,cm^{-1}$, $\alpha^2 = 0.8$, $g_\parallel/A_\parallel = 142.7\,cm^{-1}$, $K_\parallel = 0.82$, $K_\perp = 1.05$ and $K = 0.98$, ${\beta_1}^2 = 0.84$ and $\beta^2 = 1.38$, and for (**11**), are $g_\parallel = 2.28$, $g_\perp = 2.06$ and $g_{iso} = 2.13$ and $G = 4.66$ respectively, $K_\perp = 0.79$, $K_\parallel = 0.48$ and $K = 0.82$. The g-values are related by the expression [56] $G = (g_\parallel - 2)/(g_\perp - 2)$, if $G > 4.0$, then local tetragonal axes are aligned parallel or only slightly misaligned, and if $G < 4.0$, significant exchange coupling is present. Complex **10** shows a value of 3.0, indicating spin-exchange interactions take place between copper(II) ions. This is confirmed from the magnetic moment value (1.3 B.M). However, complex **11** shows a value of 4.66, indicating the presence of tetragonal axes in this complex [57, 58], in agreement with the magnetic value (1.77 B.M). Also, the $g_\parallel/A_\parallel$ values are diagnostic of

Table 4. Thermal data for the metal complexes.

| Comp. No. | Temp. (°C) | DAT (peak) Endo | DAT (peak) Exo | TGA (Wt. loss %) Calcd | TGA (Wt. loss %) Found | Assignment |
|---|---|---|---|---|---|---|
| (2) | 65 | Endo | – | 1.12 | 1.22 | Loss of hydrated water ($1/2H_2O$) |
| | 195 | Endo | – | 7.42 | 7.38 | Loss of coordinated water ($4H_2O$) |
| | 365 | Endo | – | 13.14 | 13.93 | Loss of acetate group (2) |
| | 440 | – | Exo | | | |
| | 490 | – | Exo | 18.48 | 18.85 | Decomposition of $Ni_2O_3$ |
| (4) | 80 | Endo | – | 11.02 | 11.29 | Loss of hydrated water |
| | 210 | Endo | – | 9.2 | 8.9 | Loss of coordinated water and chloride atom |
| | 310 | Endo | – | 20.2 | 20.16 | Loss of bridged chloride atom |
| | 360 | Endo | – | | | |
| | 450 | – | Exo | | | |
| | 540 | – | Exo | 39.51 | 39.43 | Decomposition with the formation of $Ni_2O_3$ |
| (7) | 230 | Endo | – | 18.33 | 17.94 | Loss of coordinated water + hydroxyl group ($7H_2O + OH$) |
| | 285 | Endo | – | 25.13 | 25.64 | Loss of coordinated bridged chloride atom (4Cl) |
| | 340 | – | Exo | | | |
| | 390 | – | Exo | | | |
| | 415 | – | Exo | | | |
| | 495 | – | Exo | | | |
| | 530 | – | Exo | 39.24 | 39.31 | Decomposition with the formation of $Co_2O_3$ |
| (10) | 50 | Endo | – | 1.18 | 1.13 | Loss of hydrated water ($1/2H_2O$) |
| | 230 | Endo | – | 9.57 | 9.43 | Loss of coordinated water ($4H_2O$) |
| | 300 | – | Exo | 9.1 | 8.96 | Loss of bridged nitrate group |
| | 370 | – | Exo | | | |
| | 470 | – | Exo | | | |
| | 520 | – | Exo | | | |
| | 545 | – | Exo | 12.94 | 12.26 | Decomposition with the formation of CuO |
| (13) | 60 | Endo | – | 2.36 | 2.27 | Loss of hydrated water ($H_2O$) |
| | 210 | Endo | – | 9.66 | 10.0 | Loss of coordinated water ($4H_2O$) |
| | 310 | Endo | – | 10.55 | 10.9 | Loss of bridged chloride atom (2) |
| | 360 | – | Exo | | | |
| | 465 | – | Exo | | | |
| | 570 | – | Exo | | | |
| | 660 | – | Exo | 26.36 | 26.36 | Decomposition with the formation of $Mn_2O_3$ |
| (15) | 65 | Endo | – | 6.84 | 6.50 | Loss of hydrated water ($2H_2O$) |
| | 140 | Endo | – | 11.02 | 11.0 | Loss of coordinated water ($3H_2O$) |
| | 280 | Endo | – | 8.14 | 8.50 | Loss of chloride atom (1) |
| | 370 | – | Exo | | | |
| | 455 | – | Exo | | | |
| | 570 | – | Exo | | | |
| | 610 | – | Exo | 39.45 | 40.0 | Decomposition with the formation of $Fe_2O_3$ |



stereochemistry [59], with square planar complexes from 105 to 135 $cm^{-1}$ and for tetragonally distorted complexes 135 to 250 $cm^{-1}$; the $g_{\|}/A_{\|}$ value for **10** (142.7 $cm^{-1}$) lies within the range expected for tetragonally distorted complexes. The $g_{\|}$-values for **10** and **11** are 2.27 and 2.28 indicating considerable covalent bonding character [30, 54, 60]. The $\sigma$-bonding parameter ($\alpha^2$) for **10** is 0.8, also suggesting covalent bonding [22, 61–63]. *K*-values for **10** and **11** are 0.98 and 0.82, respectively, confirming their covalent nature [64–66].

Complex **10** shows $\beta_1^2 = 0.48$, indicating a moderate degree of covalancy in the in-plane $\pi$-bonding, while $B^2 = 1.38$, indicating ionic character of the out-of-plane

Table 5. The percent effect of the ligand **1** and its metal complexes on microorganisms at different concentrations.

| | At 250 μg mL$^{-1}$ | | At 200 μg mL$^{-1}$ | | At 175 μg mL$^{-1}$ | | At 150 μg mL$^{-1}$ | | At 125 μg mL$^{-1}$ | |
|---|---|---|---|---|---|---|---|---|---|---|
| No. of comp. | Fungi | Bacteria | Fungi | Bacteria | Fungi | Bacteria | Fungi | Bacteria | Fungi | Bacteria |
| (1) | 0 | 12 | 0 | 0 | 0 | 0 | 0 | 0 | 0 | 0 |
| (3) | 0 | 33 | 0 | 28 | 0 | 13 | 0 | 0 | 0 | 0 |
| (4) | 0 | 37 | 0 | 25 | 0 | 12 | 0 | 0 | 0 | 0 |
| (6) | 40 | 48 | 30 | 34 | 26 | 26 | 15 | 17 | 12 | 13 |
| (7) | 39 | 46 | 29 | 32 | 15 | 25 | 0 | 16 | 0 | 11 |
| (9) | 35 | 37 | 24 | 27 | 12 | 20 | 0 | 12 | 0 | 0 |
| (10) | 35 | 39 | 25 | 32 | 13 | 20 | 0 | 13 | 0 | 0 |
| (13) | 32 | 26 | 17 | 22 | 0 | 13 | 0 | 0 | 0 | 0 |
| (14) | 37 | 45 | 29 | 31 | 17 | 24 | 0 | 15 | 0 | 0 |
| (15) | 38 | 42 | 24 | 35 | 15 | 22 | 0 | 13 | 0 | 0 |
| (16) | 35 | 36 | 23 | 27 | 12 | 13 | 0 | 0 | 0 | 0 |
| (17) | 35 | 36 | 23 | 27 | 12 | 13 | 0 | 0 | 0 | 0 |
| (18) | 35 | 36 | 23 | 26 | 12 | 12 | 0 | 0 | 0 | 0 |
| (21) | 35 | 40 | 28 | 32 | 15 | 18 | 0 | 11 | 0 | 0 |
| (22) | 15 | 18 | 12 | 14 | 0 | 0 | 0 | 0 | 0 | 0 |

The percent effect = (diameter of zone/diameter of Petri dish) × 100.
Fungi = *Aspergillus Niger*; Bacteria = *E. coli.*



$\pi$-bonding [67, 68]. It is possible to calculate approximate d orbital populations using the following equations [69],

$$A_{11} = A_{iso} - 2B\left[1 \pm \left(\frac{7}{4}\right)\Delta g_{\parallel}\right] \quad (1)$$

$$a_d^2 = \frac{2B}{2B^0} \quad (2)$$

where $2B^0$ is the calculated dipolar coupling for unit occupancy of a d orbital. When the data are analyzed using the $Cu^{63}$ hyperfine coupling, and considering all the sign combinations, the only physically meaningful results are found when $A_{\parallel}$ and $A_{\perp}$ are negative. The resulting isotropic coupling constant ($A_{iso} = -70$ G) and the parallel component of the dipolar coupling ($2B = -148$ G) are also negative. The orbital population for **10** is 63%, indicating a $d_{(x^2-y^2)}$ ground state [56]. However, the ESR spectrum of manganese(II) complex **13** is isotropic with $g_{iso} = 2.004$, typical for manganese(II) octahedral structure.

### 3.7. *Thermal analyses (DTA and TGA)*

Since the IR spectra indicate the presence of water molecules, thermal analyses (DTA and TGA) were carried out to ascertain their nature. The DTA and TGA curves show endothermic peaks within the temperature range 50–140°C, except for **7** [51, 70]. The decomposition step of **2** occurred at 65°C with 1.22% weight loss (Calcd 1.1%) due to elimination of hydrated water ($4H_2O$); for **10**, decomposition took place at 50°C with 1.13% weight loss (Calcd 1.18%), due to the loss of hydrated water ($0.5H_2O$); **13** decomposed at 60°C with 2.27% weight loss (Calcd 2.36%), corresponding to the loss of hydrated water ($H_2O$); and **15** decomposed at 65°C with 6.50% weight loss (6.84%), due

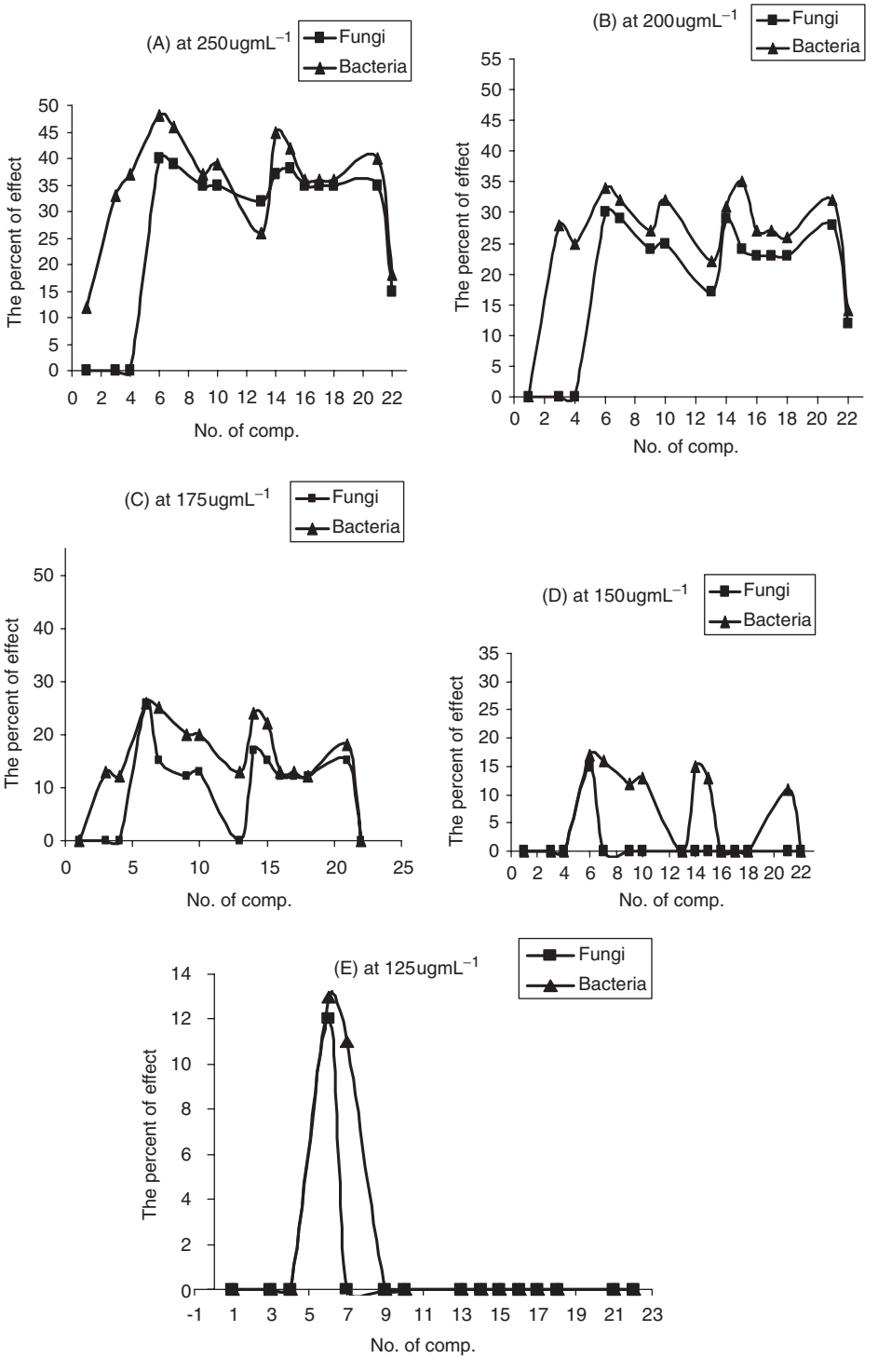




Figure 2. The percent of effect of ligand and metal complexes on microorganisms at different concentration.

to the loss of hydrated water ($5H_2O$). Another endothermic peak was observed in the 140–230°C range for **2**, **10** and **13**. For **2**, the decomposition occurred at 195°C with 7.38% weight loss (Calcd 7.42%) due to loss of four coordination water molecules; **10** at 230°C with 9.43% weight loss (Calcd 9.57%), corresponding to loss of four coordinated water molecules; **13** at 210°C with 10.0% weight loss (Calcd 9.66%), due to loss of four coordinated water molecules; **4** at 210°C with 8.9% weight loss (Calcd 9.2%), due to loss of one coordinated water and one coordinated chlorine atom; **7** showed an endothermic peak at 230°C with 17.94% weight loss (Calcd 18.33%), corresponding to the loss of seven coordinated water molecules and one hydroxyl group. The remaining thermal data are summarized in table 4. The thermal decomposition of **4** can be represented as follows:

$$[(L)(Ni)_3(H_2O)(Cl)_4]\cdot 4H_2O \xrightarrow{80^\circ C} [(L)(Ni)_3(H_2O)(Cl)_4] + 4H_2O$$

$$[(L)(Ni)_3(H_2O)(Cl)_4] \xrightarrow{210^\circ C} [(L)(Ni)_3(Cl)_3] + H_2O + Cl$$

$$[(L)(Ni)_3(Cl)_3] \xrightarrow{310,\ 360^\circ C} [(L)(Ni)_3] + 3Cl$$

$$[(L)(Ni)_3] \xrightarrow{450,540^\circ C} Ni_2O_3 + \text{volatile organic residue}$$

The thermal stability sequence is **13** > **15** > **10** > **4** > **7** > **2**.



### 3.8. *Antibacterial and antifungal screening*

The ligand and its metal complexes have been screened for their antibacterial and antifungal activities, and the results obtained are presented in table 5. Activity of the metal complexes increases with increase in the concentration of the solutions, as shown in figure 2. All the metal complexes are more potent bactericides and fungicides than the ligand [71, 72], explained on the basis of chelation theory [73, 74]. Other factors such as the nature of the metal ion, nature of the ligand, coordinating sites, and geometry of the complex, concentration, hydrophilicity, lipophilicity and presence of co-ligands have considerable influence on antibacterial activity. The mode of action of these compounds may involve hydrogen bonding through the >C=N–N=CH– group with the active centers and thus interfere with normal cell process. The presence of lipophilic and polar substituents is expected to enhance antibacterial activity. The antibacterial and antifungal activities of the hydrazone ligands and metal complexes were screened using disk diffusion [75]. The results (table 5) showed that cobalt(II) complex **6** shows higher antibacterial and antifungal activity than the other complexes. The order of activity of all the complexes is **6** > **7** > **14** > **21** > **10** > **9** > **17** = **18** > **4** > **13** > **22** > **2**. The variation in the activity of different complexes against different microorganisms depends either on the impermeability of the cells of the microbes or differences in ribosomes in microbial cells [76, 77].

## References

[1] T.D. Thangadurai, K. Natarajan. *Trans. Met. Chem.*, **27**, 840 (2002).
[2] D.X. West, A.E. Libertia, S.B. Padhye, P.B. Chikate, A.S. Sonawane. *Coord. Chem. Rev.*, **123**, 49 (1993).

[3] R.M. El-Bahnasawy, A.S. El-Tabl, E. El-Shereafy, T.I. Kashar, Y.M. Issa. *Polish J. Chem.*, **73**, 1952 (1999).
[4] D.F. Martin, G.A. Jamusonis, B.B. Martin. *J. Am. Chem. Soc.*, **83**, 73 (1961).
[5] S.K. Agrawal, R. Chandra. *Proc. Natl. Acad. Sci.*, **55**(A), 11 (1985).
[6] B. Murukan, K. Mohanan. *Trans. Met. Chem.*, **31**, 441 (2006).
[7] S.N. Pandeya, S. Smitha, M. Jyoti, S.K. Sridhar. *Acta Pharm.*, **55**, 27 (2005).
[8] A. Cukurovali, I. Yalmaz, S. Kirbag. *Trans. Met. Chem.*, **31**, 207 (2006).
[9] E.W. Ainscough, A.M. Brodie, A.J. Dobbs, J.D. Ranford, J.M. Waters. *Inorg. Chem. Acta*, **267**, 27 (1998).
[10] J.L. Buss, E. Arduini, K.C. Shephard, P. Ponka. *Biochem. Pharmacol.*, **65**, 349 (2003).
[11] S.N. Pandeya, D. Siram, G. Nath, E. Deelereg. *Eur. J. Pharm. Sci.*, **9**, 25 (1999).
[12] Y.J. Jang, U. Lee, B.K. Koo. *Bull. Korean Chem. Soc.*, **26**, 925 (2005).
[13] P. Cheng, D. Lido, S. Yan, Z. Jiang, G. Wang. *Polyhedron*, **14**, 2355 (1995).
[14] G.S. Sanyal, S. Garai. *Indian J. Chem.*, **30A**, 375 (1991).
[15] C.C. Gatto, E.S. Lang, A. Kupfer, A. Hagenbach, U. Abram. *Z. Anorg. Allg. Chem.*, **630**, 1286 (2004).
[16] Maged. Mohammed. Ahmed. Azzam, M.Sc. Thesis, Faculty of Science, Menoufia University, Egypt (2005).
[17] A. Earnshaw. *Introduction to Magneto Chemistry*, p. 4, Academic Press, London (1968).
[18] J. Patole, U. Sandbhor, S. Padhye, D.N. Deobagkar, C.E. Anson, A. Powell. *Bioorg. Med. Chem. Lett.*, **13**, 51 (2003).
[19] K.B. Gudasi, S.A. Patil, R.S. Vadvavi, R.V. Shenoy, M. Nethaji. *Trans. Met. Chem.*, **31**, 586 (2006).
[20] K.B. Gudasi, M.S. Patel, R.S. Rashmi, V. Shenoy, S.A. Patil, M. Nethaji. *Trans. Met. Chem.*, **31**, 580 (2006).
[21] A.S. El-Tabl, R.M. Issa. *J. Coord. Chem.*, **57**, 509 (2004).
[22] A.S. El-Tabl. *Trans. Met. Chem.*, **22**, 400 (1997).
[23] A. Cukurovali, I. Yilmas. *Trans. Met. Chem.*, **31**, 207 (2006).
[24] A.S. El-Tabl, T.I. Kasher, R.M. El-Bahnaswy, A.E. Ibrahim. *Polish J. Chem.*, **73**, 245 (1999).
[25] H.A. El-Boraey, A.S. El-Tabl. *Polish J. Chem.*, **77**, 1759 (2003).
[26] L. Mishra, A. Jha, A.K. Yadaw. *Trans. Met. Chem.*, **22**, 406 (1997).
[27] A.S. El-Tabl, K. El-Baradie, R.M. Issa. *J. Coord. Chem.*, **56**, 1113 (2003).
[28] W.H. Hegazy. *Monatsh. Chem.*, **132**, 639 (2001).
[29] K. Nakamato. *Infrared and Raman Spectra of Inorganic and Coordination Compounds*, 4th Edn, Wiley Interscience, New York (1986).
[30] N. Raman, A. Kulandaisamy, C. Thangaraja, P. Manisankar, S.V. Swanathan, C. Vedhi. *Trans. Met. Chem.*, **29**, 129 (2004).
[31] A.S. El-Tabl. *Trans. Met. Chem.*, **27**, 166 (2002).
[32] P. Athappan, G. Rajagopal. *Trans. Met. Chem.*, **22**, 84 (1997).
[33] A.S. El-Tabl. *J. Chem. Res. (S)*, 529 (2002); *J. Chem. Res. M*, 1110 (2002).
[34] S.D. Robenson, M.F. Uttly. *J. Chem. Soc. Dalton Trans.*, 1912 (1973).
[35] K. Nakamato. edn. *Infrared Spectra of Inorganic and Coordination Compounds*, 2nd Edn, Wiley Interscience, Inc., New York (1967).
[36] J.R. Ferraro, W.R. Walker. *Inorg. Chem.*, **4**, 1382 (1965).
[37] H.M. El-Tabl, F.A. El-Said, M.I. Ayad. *Synth. React. Inorg. Met.-Org. & Nano-Met. Chem.*, **35**, 243 (2005).
[38] R.A. Lal, A. Kumar. *Ind. J. Chem.*, **38A**, 839 (1999).
[39] A. El-Motaleb, M. Ramadan, W. Sawodny, H.F. El-Baradie, M. Gaber. *Trans. Met. Chem.*, **22**, 211 (1997).
[40] J.K. Nag, S. Pal, C. Sinha. *Trans. Met. Chem.*, **30**, 523 (2005).
[41] A.S. El-Tabl, M.I. Ayad. *Synth. React. Inorg. Met.-Org. Chem.*, **33**, 369 (2003).
[42] D.N. Sathyanarayana. *Electronic Absorption Spectroscopy and Related Techniques*, Orient Longman Limited © Universities Press (India) Limited, India (2001).
[43] A.S. El-Tabl, S.A. El-Enein. *J. Coord. Chem.*, **57**, 281 (2004).
[44] A. Cukurovali, I. Yalmaz, S. Kirbag. *Trans. Met. Chem.*, **31**, 207 (2006).
[45] C.H. Krishna, C.M. Mahapatra, K.C. Dush. *J. Inorg. Nucl. Chem.*, **39**, 1253 (1977).
[46] R. Atkins, G. Brewer, E. Kokot, G.M. Mockier, E. Sinn. *Inorg. Chem.*, **24**, 127 (1985).
[47] S.A. Sallam, A.S. Orabi, B.A. El-Shetary, A. Lentz. *Trans. Met. Chem.*, **27**, 447 (2002).
[48] R.K. Parihari, R.K. Patel, R.N. Patel. *J. Ind. Chem. Soc.*, **77**, 339 (2000).
[49] N.K. Singh, S.B. Singh. *Trans. Met. Chem.*, **26**, 487 (2001).
[50] K. Nehru, P. Athappan, G. Rajagopal. *Trans. Met. Chem.*, **26**, 652 (2001).
[51] A.S. El-Tabl, R.M. Issa, M.A. Morsi. *Trans. Met. Chem.*, **29**, 543 (2004).
[52] G. Knör, A. Strasser. *Inorg. Chem. Commun.*, **8**, 471 (2005).
[53] B.D. Wang, Z.Y. Yang, Q. Wang, T.K. Cai, P. Crewdson. *Bioorg. Med. Chem.*, **14**, 1880 (2006).
[54] A.S. EL-Tabl. *Bull. Korean Chem. Soc.*, **25**, 1 (2004).
[55] A.S. EL-Tabl. *Trans. Met. Chem.*, **21**, 428 (1996).

[56] A.S. EL-Tabl. *Trans. Met. Chem.*, **23**, 63 (1998).
[57] I.M. Procter, B.J. Hathaway, P. Nicholls. *J. Chem. Soc. A*, 1678 (1969).
[58] A.S. EL-Tabl. PhD. Thesis, Menoufia University, Egypt (1993).
[59] A.A.G. Tomlinson, B.J. Hathaway. *J. Chem. Soc. A*, 1905 (1968).
[60] D. Kivelson, R. Neiman. *J. Chem. Phys.*, **35**, 149 (1961).
[61] H.A. Kuska, M.T. Rogers. In *Coordination Chemistry*, A.E. Martell (Ed.), Van Nostrand Reinhold, New York (1971).
[62] B.R. McGarvey. *Trans. Met. Chem.*, **3**, 89 (1966).
[63] R.K. Ray. *Inorg. Chim. Acta*, **174**, 237 (1990).
[64] R.K. Ray. *Inorg. Chim. Acta*, **174**, 257 (1990).
[65] J.M. Assour. *J. Chem. Phys.*, **43**, 2477 (1965).
[66] S.E. Harrison, J.M. Assour. *J. Chem. Phys.*, **40**, 365 (1964).
[67] Z.W. Mao, K.B. Yu, D. Chen, S.Y. Han, Y.X. Sui, W.X. Tang. *Inorg. Chem.*, **32**, 2140 (1993).
[68] M.M. Bhabbhade, D. Srinivas. *Inorg. Chem.*, **32**, 5458 (1993).
[69] M.C.R. Symons. *Chemical and Biochemical Aspects of Electron Spin Resonance*, Van Nostrand Reinhold, Wokingham (1979).
[70] A.S. El-Tabl, S.M. Imam. *Trans. Met. Chem.*, **22**, 259 (1997).
[71] D. Sriram, P. Yogeeswari, R.V. Devakaram. *Bioorg. Med. Chem.*, **14**, 3113 (2006).
[72] S.K. Sridhar, M. Saravanan, A. Ramsh. *Eur. J. Med. Chem.*, **36**, 615 (2001).
[73] K.N. Thimmaiah, W.D. Lioyd, G.T. Chandrappa. *Inorg. Chim. Acta*, **106**, 81 (1985).
[74] T.J. Franklin, G.A. Snow. *Biochemistry of Antimicrobial Action*, 2nd Edn, Chapman and Hall, London (1971).
[75] C.H. Collins, P.M. Lyn. *Microbial Methods*, University Park Press, Baltimore (1970).
[76] M. Kurtoġlu, E. Ispir, N. Kurtoġlu, S. Toroġlu, S. Serin. *Trans. Met. Chem.*, **30**, 765 (2005).
[77] M. Kurtoġlu, M.M. Daġdelen, S. Toroġlu. *Trans. Met. Chem.*, **31**, 382 (2006).